# Holographic fabrication of graded photonic super-crystals through pixel-by-pixel phase coding of laser beams in a spatial light modulator

Oliver Sale<sup>a,\*</sup>, Safaa Hassan<sup>a</sup>, David Lowell<sup>a</sup>, Noah Hurley<sup>a</sup>, Yuankun Lin<sup>a,b</sup>
<sup>a</sup>Department of Physics, Univ. of North Texas, Denton, TX, USA 76203
<sup>b</sup>Department of Electrical Engineering, Univ. of North Texas, Denton, TX, USA 76203
\*oliversale@my.unt.edu

#### **ABSTRACT**

This paper presents a holographic fabrication of a new type of photonic crystal, called graded photonic super-crystals with graded basis, dual period and dual symmetry. Pixel-by-pixel phase coding of laser beams in a spatial light modulator can produce the highest resolution in produced photonic super-lattice. Two-level designs in phase pattern are used to generate graded photonic super-crystals where graded square lattice clusters are orientated in four, five or six-fold symmetry. Further phase engineering in a super-cell of 12x8 pixels can produce small-period square lattice orientated in a large period rectangular pattern.

**Keywords**: photonic crystals; graded photonic super-crystals; photonic quasi-crystal; holographic lithography; spatial light modulator

### 1. INTRODUCTION

Photonic crystals have been studied for their integration in enhanced light-matter interaction, photonic band gap engineering, and in functional optical devices [1–3]. First generation two-dimensional (2D) photonic crystals were uniform in their lattice [4], as depicted by the regions inside the solid blue rectangle in Figure 1. With the second generation, these 2D photonic crystals were made of dual lattices, the first (second) represented by the green (purple) dots in Figure 1. Furthermore, these photonic crystals have been found to have enhanced light-matter interactions [5,6]. Recently, we have studied a new type of photonic crystal termed graded photonic super-crystals (GPSC) [7–11] as well as graded photonic super-quasi-crystals [12-18]. The lattice for GPSC is grouped similarly to the second generation 2D photonic crystals, while, photonic quasi-crystals form super-lattices about rotational symmetry instead of translational. Moreover, the GPSC and graded photonic super-quasi-crystals by the size of the basis. Specifically, the basis size is a gradient, decreasing in size along the purple and green arrows in Figure 1, and then increasing after a quarter period. Therefore, the original unit cell of a traditional photonic crystal forms a larger unit super-cell in the GPSC and a larger unit super-quasi-crystal in the graded photonic super-quasi-crystal. The original period which we will name "Period 1" and the unit super-cell period described by "Period 2" are shown in their respective x-directions in Figure 1(a). While the lattice of Period 1 has square symmetry, the lattice cluster indicated by the dashed blue rectangle can have a square or five-fold symmetry as shown in Figure 1(a) and 1(b), respectively. Period 1 can have other symmetries, though, these reduce resolution in phase pattern while using a spatial light modulator (SLM) for fabrication [7–11]. Lastly, in the GPSC and graded photonic super-quasicrystals the filling fraction of the dielectric material is also gradient. The region contained in the dashed green rectangular region has a high filling fraction, while the region in the solid blue rectangle has a low filling fraction.

Multiple-beam-based interference lithography has been used successfully for the fabrication of a photonic crystal template [19–26]. To improve the mechanical stability of the optical setup and reduce the complexity a phase mask or single reflection optical element has been utilized [17,18,27–31]. More recently, a SLM has been used as an electrically adjustable phase mask [17,18,27–32]. Via the use of the computer-generated hologram method, pixel-by-pixel phase engineering in the SLM can reach a high resolution in the holographic fabrication [7,10,11,31,32]. In addition, the Fourier filter can be predicted, and the reflective optical element can be used which allows for a larger area holographic fabrication [10]. Via the pixel-by-pixel phase engineering method, graded photonic super-crystals with square [7], five-fold [11], and hexagonal [7] symmetric unit super-cells have been fabricated. These structures were fabricated with by four outer beams with large interfering angles, plus four, five, and six inner beams with small interfering angles respectively [7,11]. With a single reflective optical element, the interfering angles of the four outer beams common to all structures can be increased to fabricate graded photonic super-crystals with a small Period 1 [10].

In this paper, we have studied the holographic fabrication of graded photonic super-crystals with a rectangular unit super-cell and of photonics quasi-crystals with five-fold symmetry. A rectangular and 5-fold unit super-cell in a phase pattern are designed to have a desired ratio of length over width and triangular lengths, respectively, via the same experimental setup.

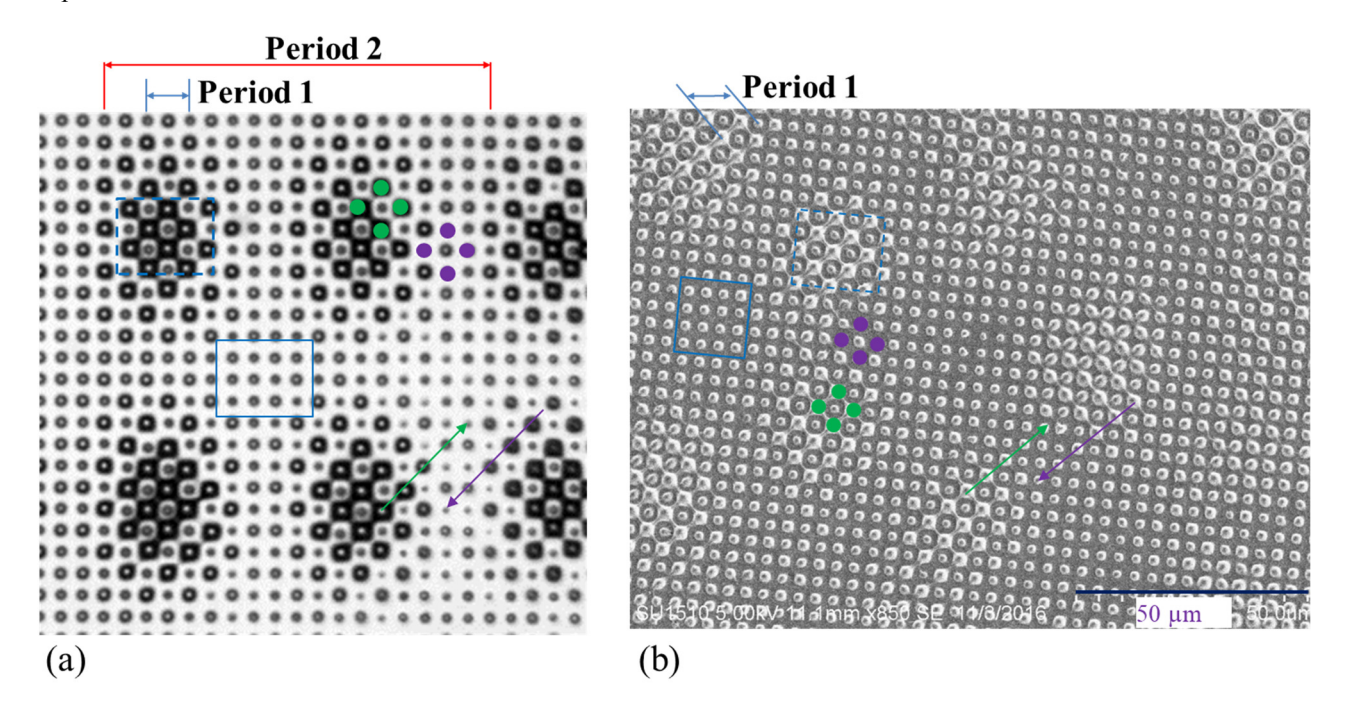


Figure 1. (a) Image of a graded photonic super-crystals: the lattices can be grouped by green and purple dots. The size of the basis becomes smaller along the green and purple arrows and then becomes larger after a quarter of "Period 2". The filling fraction of the dielectric material is higher inside the dashed blue rectangle than the solid blue rectangle. The graded photonic super-crystals have a unit super-cell as indicated by Period 2 in the x-direction. (b) Image of a photonic quasicrystal: the lattices are grouped by green and purple dots. The size of the basis becomes smaller along the green and purple arrows and then becomes larger. The filling fraction of the dielectric material is higher inside the dashed blue rectangle than the solid blue rectangle.

# 2. DESCRIPTION OF EXPERIMENTAL METHODS AND FORMATION OF GPSC AND GRADED PHOTONIC SUPER-QUASI-CRYSTAL

A 532 nm laser beam (Cobolt Samba 50 mW) was expanded and collimated using lenses and a spatial filter. The phase of the laser beam was modulated using the engineered phase pattern displayed in a phase-only SLM (Holoeye PLUTO). It has an active area of  $15.36 \times 8.64$  mm<sup>2</sup> with  $1920 \times 1080$  pixels. The pixel size of the SLM is  $8 \times 8$   $\mu$ m<sup>2</sup> ("P" is the side length of a pixel square = 8  $\mu$ m, which has been used in this paper). The laser is linearly polarized along the longer side of the active area and is incident onto the SLM with an incident angle of four degrees, relative to the normal of the SLM. As shown in Figure 2, the diffracted beams from the phase pattern (Figure 3(a1,a2)) are displayed in the SLM and are collected

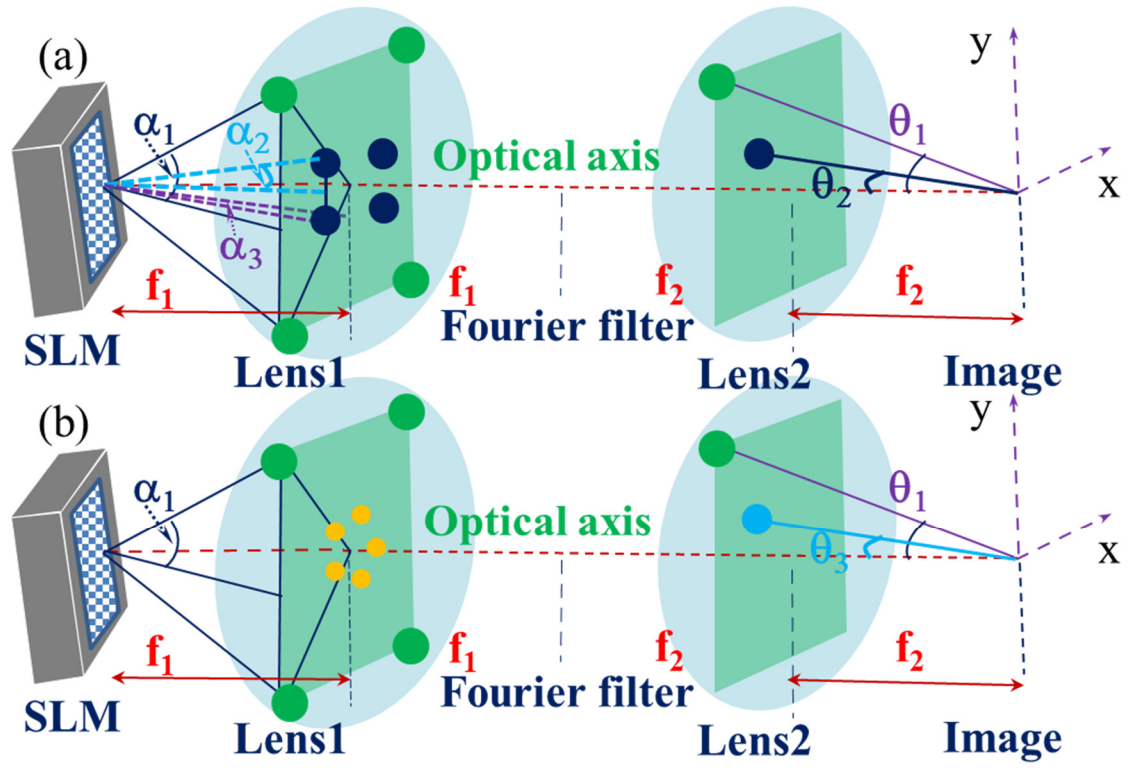


Figure 2. (a) Schematic of the optical setup for the holographic fabrication. The spatial light modulator (SLM) is used to display the phase patterns. The diffracted beams from the SLM are filtered at the Fourier plane and form interference patterns through a 4f imaging system of lens 1 and lens 2.  $\alpha_1$ ,  $\alpha_2$ , and  $\alpha_3$  are the first order diffraction angles due to the periodic array of 2P ("P" is the side length of a pixel square = 8  $\mu$ m, which has been used in this paper) pixels in x and y directions, 24P pixels in y-direction, and 18P pixels in x-direction in the phase pattern in, respectively.  $\theta_1$  and  $\theta_2$  (zenith angle) are the interfering angles of the outer beam and inner beams, respectively. (b) Schematic of the optical setup for the holographic fabrication. The SLM is used to display the phase patterns. The diffracted beams from the SLM are filtered at the Fourier plane and form interference patterns through a 4f imaging system of lens 1 and lens 2.  $\alpha_1$  is the first order diffraction angle due to the periodic array of 2P ("P" is the side length of a pixel square = 8  $\mu$ m, which has been used in this paper) pixels in x and y directions, 48P pixels in y-direction, and 46P pixels in x-direction in the phase pattern in, respectively.  $\theta_1$  and  $\theta_3$  are the interfering angles of the outer beam and inner beams, respectively.

The rectangular unit super-cell of the phase pattern is indicated by a dashed blue square in Figure 3(a1). The unit super-cell was divided into two  $12 \times 12$  checkerboard regions (dashed red) and two  $12 \times 6$  checkerboard regions (dashed blue). The gray levels of (190 and 254) are used for the regions inside the dashed red and green squares, while (128 and 254) are used for the regions outside of the dashed squares in the unit super-cell. The decagonal unit

super-cell of the phase patter is indicated by a dashed red triangle in Figure 3(a2). Figure 3(a3) represents the geometry of one of the triangular regions of the unit super-cell. In order to form the triangle, the lengths of A (dashed red line), B (solid green line), and C (dotted blue line) must satisfy  $A = B/\cos(18^{\circ})$  and  $C = 2B \tan(18^{\circ})$  where A, B, and C are in units of P. Figure 3(a2) has a side length of 2A and a width of 2B, thus, to integrate some degree of desired disorder in the fabricated 5-fold graded photonic super-quasi-crystal (A,B,C) were set to (24, 23, 15). The unit super-cell in Figure 3(a2) was divided into ten alternating triangles as described by the geometry of Figure 3(a3) with gray levels of (192 and 254) for the dashed red area and of (158 and 254) for the dashed green area. The gray levels for both unit super-cells were selected individually based on the diffraction efficiency of a small-period pattern verse a large-period pattern, their ratio, and the formation of a graded photonic super-crystals through simulation [7,11]. A simulation of an interference pattern of multi-beams with measured diffraction efficiencies and a certain exposure threshold was used to determine the gray level selection [11]. A gamma curve modulated a  $0\pi$  and  $2\pi$  phase into the laser beam when it as reflected by a gray level of 0 and 255, respectively, and related the phase and gray level almost linearly between 0 and 255. A gray level of 190 corresponds to a phase of  $(190 \times 2\pi/255)$ . A gray level of 254 was typically used instead of 255 because 255 corresponds to  $2\pi$  or  $0\pi$  in the cosine function in the simulation.

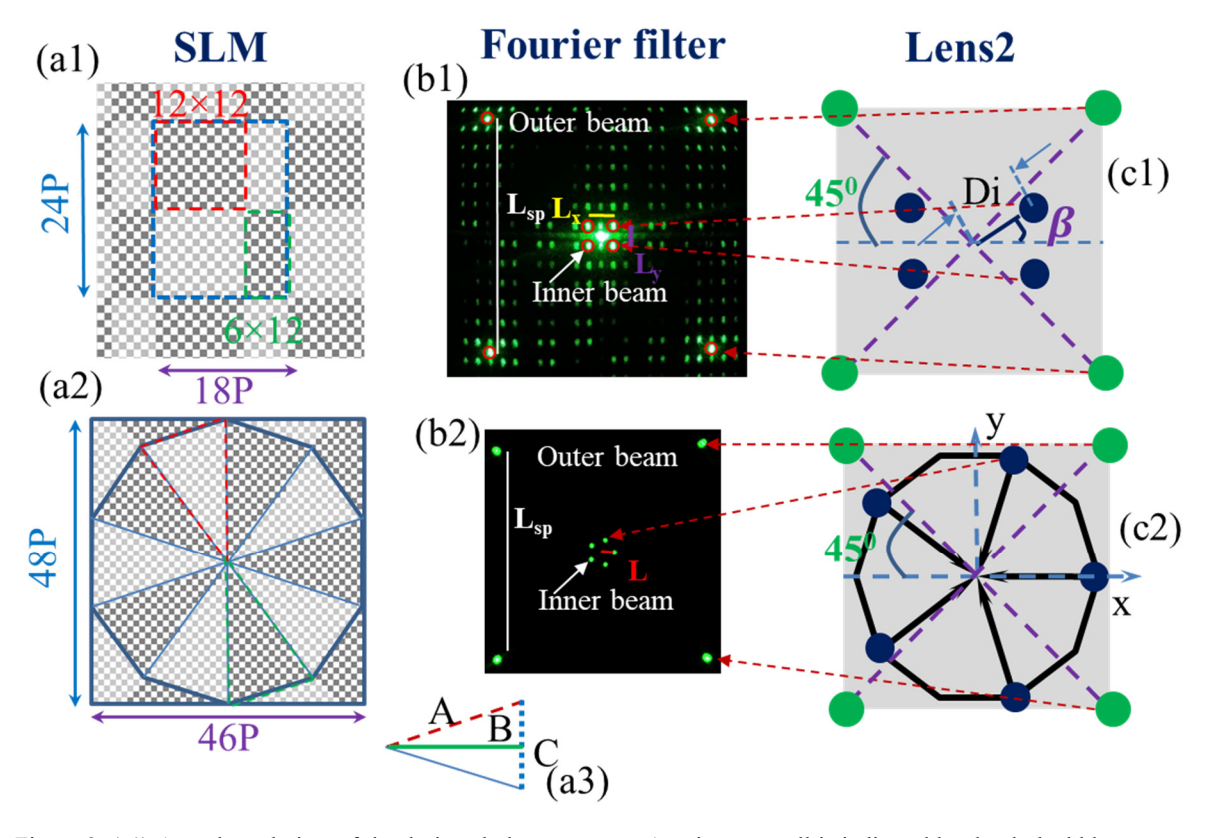


Figure 3. (a1) An enlarged view of the designed phase patterns. A unit super-cell is indicated by the dashed blue square. Inside the unit-cell, there are two  $12 \times 12$  square pixel patterns (dashed red) and two  $12 \times 6$  square pixel patterns (dashed green). The gray levels of (190 and 254) correspond to the dashed red and green regions, while (128 and 254) correspond to the remaining regions inside the unit super-cell. (b1) The laser diffraction pattern from the phase pattern in (a1) at the Fourier plane. A Fourier filter is used to allow the diffraction spots inside the red circles passing through. (c1) Schematic of eight beams corresponding to the outer and inner beams in (b1) for the interference lithography.  $\beta$  is an azimuthal angle for one of the inner beams in (b1). (a2) An enlarged view of the designed phase patterns. A unit super-cell is indicated by the decagon outlined in blue. Inside the unit-cell, are alternating triangles of gray levels of (158, 254) for the red dashed area and (192, 254) for the green dashed area. (a3) Schematic of one of the triangles of the decagon. (b2) Optical image of the diffraction pattern taken after the Fourier filter. (c2) The configuration of 4 + 5 interference with four outer beams and five inner beams.

When the 532 nm laser is the incident onto the phase pattern in the SLM, it is diffracted using the following equation:

$$D \times \sin \alpha_i = n\lambda, \quad i = 1, 2, 3 \tag{1}$$

where D is the structural period;  $\alpha$  the first order diffraction angle, as defined in Figure 2 and described below; and n is the diffraction order. Furthermore,  $\alpha_1$  is the first order diffraction angle due to the periodic array of the gray levels of (128 and 254) or (190 and 254) for the rectangular unit super-cell and (158 and 254) or (192 and 254) for the 5-fold unit super-cell. Respectivley,  $\alpha_1$  can be obtained by setting D=2P or D=B in Equation (1). For a large period in x- and y-directions, D in Equation (1) equals 23P for the 5-fold unit super-cell and 18P and 24P for the rectangular unit super-cell where  $\alpha_1$  equals  $\alpha_3$  and  $\alpha_2$ , respectively. The distance  $L_{\rm sp}$ ,  $L_{\rm x}$ , and  $L_{\rm y}$  due to the small period 2P arrays between the  $\pm 1$  order diffractions, 18P arrays in the x-direction, and 24P arrays in the y-direction, and can be measured in Figure 3(a1-c1), respectively. While the distance  $L_{\rm sp}$  due to the outer order  $\pm 1$  diffractions and L due to the inner order diffractions from optical axis can be measured in Figure 3(a2-c2). The diffraction condition in Equation (1) was tested by verifying  $L_{\rm sp} = 2 \times f_1 \tan(\alpha_1)$ ,  $L_{\rm x} = 2 \times f_1 \tan(\alpha_3)$ , and  $L_{\rm y} = 2 \times f_1 \tan(\alpha_2)$ , as shown in Figure 2(a) and Figure 3(b1), and by verifying  $L = 2 \times f_1 \tan(\alpha_1)$ , as shown in Figure 2(b) and Figure 3(b2). Theoretically, for the rectangular diffraction pattern  $L_{\rm sp}/L_{\rm x} = 9$  and  $L_{\rm sp}/L_{\rm y} = 12$  and for the 5-fold diffraction pattern L = 2.05. As measured, in Figure 3(b1),  $L_{\rm xp}/L_{\rm x} = 9.20$  and  $L_{\rm sp}/L_{\rm y} = 12.23$  and in Figure 3(b2) L = 2.07. The agreement between the measured and theoretical values is high, indicating the correct assignment for D.

In the experimental setup, the lenses with focal lengths of  $f_1$  = 400 mm and  $f_2$  = 200 mm for lens 1 and lens 2, respectively, were used. The 4f setup, as shown in Figure 2, was used for both. The graded photonic super-crystal and the graded photonic super-quasi-crystal were fabricated by exposing the dipentaerythritol penta/hexaacrylate (DPHPA) mixture to the inference pattern with similar spin-coating, exposure, and development conditions, as in reference [7,10,11].

#### 3. RESULTS

The intensity, I(r), of the multiple beam interference pattern is determined by the following:

$$I(r) = \langle \sum_{i=1}^{m} E_i^2(r,t) \rangle + \sum_{i \leq j}^{m} \mathbf{E}_i \cdot \mathbf{E}_j \cos[(k_j - k_i) \cdot r + (\varphi_j - \varphi_i)].$$
 (2)

where E is the electric field; k is the wave vector;  $\phi$  is the initial phase of the beam.

## 3.1 Holographic Fabrication Results of GPSC

Due to the symmetry of the eight beams allowed to pass through by the Fourier filter for the GPSC, detailed in red circles in Figure 3(b1), the beams can be easily represented by the following equations:

$$\mathbf{E}_1(r,t) = \mathbf{E}_1 \cos[+(k\sin\theta_1\cos45)x + (k\sin\theta_1\sin45)y + (k\cos\theta_1)z - \omega t + \varphi_1] \tag{3}$$

$$\mathbf{E}_{2}(r,t) = \mathbf{E}_{2}\cos[-(k\sin\theta_{1}\cos45)x + (k\sin\theta_{1}\sin45)y + (k\cos\theta_{1})z - \omega t + \varphi_{2}] \tag{4}$$

$$\mathbf{E}_3(r,t) = \mathbf{E}_3 \cos[-(k\sin\theta_1\cos45)x - (k\sin\theta_1\sin45)y + (k\cos\theta_1)z - \omega t + \varphi_3] \tag{5}$$

$$\mathbf{E}_{4}(r,t) = \mathbf{E}_{4}\cos[+(k\sin\theta_{1}\cos45)x - (k\sin\theta_{1}\sin45)y + (k\cos\theta_{1})z - \omega t + \varphi_{4}] \tag{6}$$

$$\mathbf{E}_{5}(r,t) = \mathbf{E}_{5}\cos[+(k\sin\theta_{2}\cos\beta)x + (k\sin\theta_{2}\sin\beta)y + (k\cos\theta_{2})z - \omega t + \varphi_{5}] \tag{7}$$

$$\mathbf{E}_{6}(r,t) = \mathbf{E}_{6}\cos[-(k\sin\theta_{2}\cos\beta)x + (k\sin\theta_{2}\sin\beta)y + (k\cos\theta_{2})z - \omega t + \varphi_{6}] \tag{8}$$

$$\mathbf{E}_{7}(r,t) = \mathbf{E}_{7}\cos[-(k\sin\theta_{2}\cos\beta)x - (k\sin\theta_{2}\sin\beta)y + (k\cos\theta_{2})z - \omega t + \varphi_{7}] \tag{9}$$

$$\mathbf{E_8}(r,t) = \mathbf{E_8}\cos[+(k\sin\theta_2\cos\beta)x - (k\sin\theta_2\sin\beta)y + (k\cos\theta_2)z - \omega t + \varphi_8] \tag{10}$$

where  $\theta_1$  and  $\theta_2$  (zenith angle) are the interfering angles of the outer beam and inner beams, respectively, in Figure 2(a) and Figure 3(b1-c1); 45° and  $\beta$  are the azimuthal angles for outer and inner beams respectively.

Via MATLAB, the Equations (2)–(10) produced the interference pattern shown in Figure 4(a). The eight-beam interference can also be approximately understood by adding the interference of beams 1–4 to the beams 5–8. The inference of beams 1–4 forms a structure with a small period of  $\Lambda_s = 2\pi/(k\sin(\theta_1)\cos(45))$ , where  $\theta_1$  is determined by  $\tan(\theta_1) = f_1\tan(\alpha_1) \times \sqrt{2}/f_2$ . Thus,  $\Lambda_s = (f_2/f_1)2P$ . The period  $\Lambda_x$  in the x-direction in the interference among beams 5-8 is different from period  $\Lambda_y$  in the y-direction, and are calculated as follows:  $\Lambda_x = 2\pi/(k\sin(\theta_2)\cos(\beta))$  and  $\Lambda_y = 2\pi/(k\sin(\theta_2)\sin(\beta))$ , where  $\sin(\theta_2)\cos(\beta) \simeq (Di/f_2)(0.5 L_x/Di)$  and  $\sin(\theta_2)\sin(\beta) \simeq (Di/f_2)(0.5 L_y/Di)$ , as shown in Figure 2(c,d). Thus,  $\Lambda_x = (f_2/f_1)18P$  and  $\Lambda_y = (f_2/f_1)24P$ .

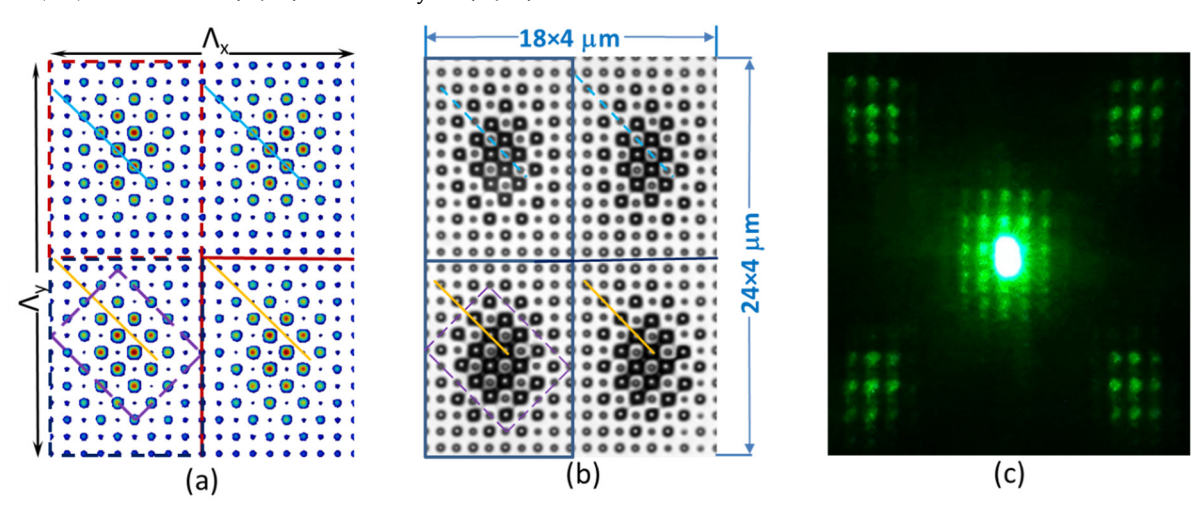


Figure 4. (a) Simulated eight-beam interference pattern; (b) the charge-coupled device (CCD, attached to an optical microscope) image of the fabricated graded photonic super-crystal in dipentaerythritol penta/hexaacrylate (DPHPA); (c) diffraction pattern of a fabricated sample from 532 nm laser.

A simulated eight-beam interference pattern, as shown in Figure 4(a), assumes the same initial phase for all eight beams in Equation (10). The periodicity in the x- and y-directions ( $\Lambda_x$ ,  $\Lambda_y$ ) is labeled for the size of the unit super-cell in the holographic structure in Figure 4(a). Despite that both the square (12 × 12) and rectangular (6 × 12) sub-unit cells are present in Figure 3(a1), the sub-unit cell has a rectangular shape, as indicated by the dashed red line in Figure 4(a). The unit super-cell in Figure 4(a) has a ratio of length over width given by  $\Lambda_y/\Lambda_x = 24/18$ , given by (12 + 12)/(12 + 6) as depicted in Figure 3(a1). Moreover, the design of the phase pattern is flexible. For example, the unit super-cell in the phase pattern can have a sub-unit of k × k and k × m pixels. This would give the obtained holographic structure defined by a rectangular unit super-cell with a ratio of side lengths defined by 2k/(k + m).

Figure 4(b) shows a charge-coupled device (CCD, attached to the optical microscope) image of the fabricated graded photonic super-crystals in DPHPA. Figure 4(b) demonstrates the graded pattern and dual periodicity (one in 4  $\mu$ m and the others in 18 × 4  $\mu$ m and 24 × 4  $\mu$ m). The fabricated pattern has a unit super-cell indicated by a dashed red rectangle with a size of (18 × 4  $\mu$ m) × (24 × 4  $\mu$ m). The super-cell can be divided into four sub-units, dictated by the blue square in Figure 4(b), which correspond to the sub-unit dictated by the dashed red rectangle in simulation in Figure 4(a). The lattice has a small period of 4  $\mu$ m for both the x and y-directions. The graded lattice clusters have a rectangular symmetry. Thus, we have a graded photonic super-crystal with square lattices and rectangular lattice clusters.

The diffraction pattern of the fabricated sample is shown in Figure 4(c), using a 532 nm laser. Near the 0th order diffraction spot, there are several high order diffractions. In the four corners, there are more than nine diffraction spots in each, due to the small periodic lattice and graded feature. The multiple-order diffraction indicates not only the quality of the fabricated sample but also the strong light-matter interaction, which can be used for light extraction.

#### 3.2 Holographic Fabrication Results of Graded Photonics Super-Quasi-Crystal

The graded photonic super-quasi-crystal shares the same four outer beam (Equations (3-6)) structure as the GPSC, however, the inner beam structure is described by the following equations:

$$\mathbf{E}_{5-9}(r,t) = \mathbf{E}_{5-9} \cos[k_a \cdot r - \omega t + \varphi_{5-9}] \tag{11}$$

The five inner wavevectors  $k_q$  in Eq. (11) can be described by the following equation:

$$k_q = k \left( \sin \theta_3 \cos \frac{2(q-1)\pi}{5}, \sin \theta_3 \sin \frac{2(q-1)\pi}{5}, \cos \theta_3 \right), \qquad q = 1, 2, ..., 5$$
 (12)

where  $\theta_3$  is defined in Fig. 2(b).

The Equations (2)-(6),(11-12) were programed into MATLAB, which produced the interference pattern in Figure 5(a). The nine-beam interference can be approximately understood by adding the interference of beams 1–4 to the beams 5–9. The inference of beams 1–4 forms a structure with a small period of  $\Lambda_s = 2\pi/(k\sin(\theta_1)\cos(45))$ , where  $\theta_1$  is determined by  $\tan(\theta_1) = f_1\tan(\alpha_1) \times \sqrt{2}/f_2$ . Considering  $\tan(\theta) \simeq \sin(\theta)$  for small angle,  $\Lambda_s = ((1 \text{ pixel length}))/2$ . Thus, the small period  $\Lambda_s$  is 4  $\mu$ m as confirmed by the scanning electron microscope (SEM) measurements [11]. Interference between two of the inner beams is indicated by the solid blue line in Figure 5(b) and described by  $k_q - k_{q-2}$ . The set of  $k_q - k_{q-2}$  forms a circle in the generated holographic structure indicated by the dashed blue line in Figure 5(b) with a radius  $R_2 = 2\pi/(k_q - k_{q-2})$ . Thus,  $R_2 = 12.1 \times 4 \mu$ m. Moreover, inside the dashed blue circle in Figure 5(b), the graded pattern has five-fold symmetry as indicated by the solid red decagon; the holographic graded super-lattice appears alternating in the decagon.

As the graded photonic super-quasi-crystal lacks translational symmetry, other regions of the fabricated sample could have different symmetry, Figure 5(c) is one such example. The interference in the region indicated by the dashed blue lines if defined by  $k_q - k_{q-1}$ . The set of  $k_q - k_{q-1}$  form a circle indicated by the purple circle in Figure 5(c) and defined by radius  $R_1 = 2\pi/(k_q - k_{q-1})$ . Thus  $R_1 = 19.6 \times 4$  µm. The purple circle is centered on a graded lattice. Inside the purple circle, ten graded regions are indicated by the vertices of the red decagon as shown in Figure 5(c). The decagon structure has also been observed in conventional photonic quasi-crystals [33]. Pre-designed disorder is visible in Figure 5(c), as two graded regions are overlapped in the left side of the decagon.

Figure 5(d) shows the diffraction pattern of a 532 nm laser from the fabricated sample of the graded photonic super-quasi-crystal. The square symmetry from the small periodicity is indicated by the four patterns at the four corners in the Fig. 5(d). The quasi-crystal generates ten-fold symmetric diffraction spots. In the figure, the ten-fold spots form the first-order (the strongest), the second-order, and the third-order (the weakest) ring structures. The ratios of the second-order ring diameter to that of the first-order ring and the third-order

ring diameter to that of the second-order ring were measured to be 1.609 and 1.610, respectively, close to theoretical value of 1.618 (golden ratio [34,35]), further confirming the five-fold symmetry in the fabricated sample.

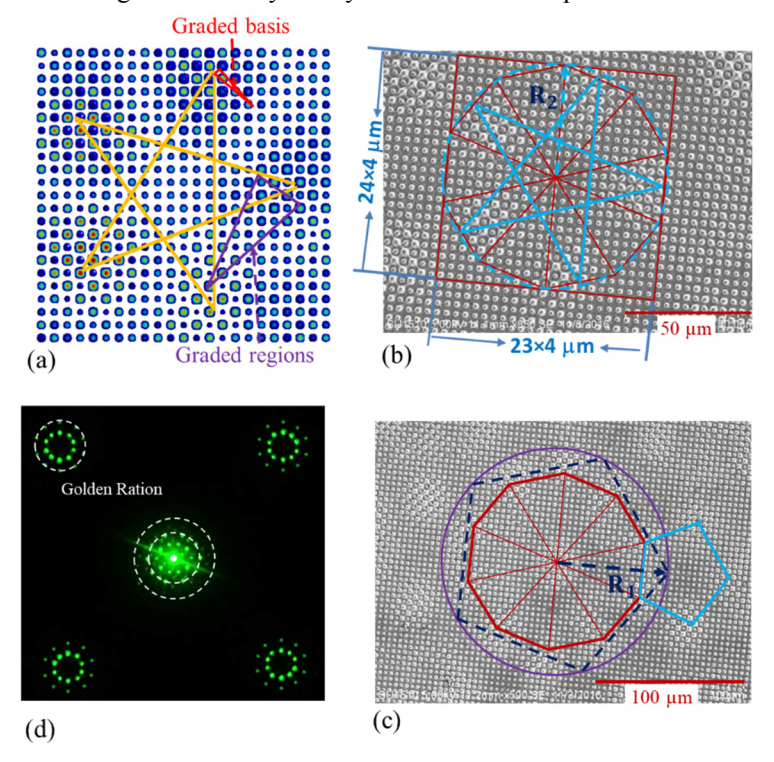


Figure 5. (a) Simulated eight-beam interference pattern; (b) Scanning Electron Microscope (SEM) image of a fabricated sample in one area where the graded regions have five-fold symmetry due to the interference of individual beams with their next-neighbor beams as indicated by the solid yellow lines. The graded basis and graded regions are highlighted; (c) SEM image of a fabricated sample in another area where the graded regions are a result from the interference of individual beams with their neighboring beams as indicated by the solid yellow lines; (d) diffraction pattern of a fabricated sample from 532 nm laser.

#### 4. CONCLUSION

A graded photonic super-crystal and a graded photonic quasi-super-crystal have been holographically fabricated via pixel-by-pixel phase engineering in a SLM. The phase pattern design in the SLM has shown to be effective in creating a graded photonic super-crystal with a desired length over width in the rectangular super-cell and a graded photonic quasi-super-crystal with the desired disorder in the 5-fold symmetric super-cell.

Funding: This research was funded by U.S. National Science Foundation, grant number 1661842.

#### REFERENCES

- [1] Tandaechanurat, A., Ishida, S., Guimard, D., Nomura, M., Iwamoto, S., and Arakawa, Y., "Lasing oscillation in a three-dimensional photonic crystal nanocavity with a complete bandgap," Nat. Photonics 2011, 5, 91–94.
- [2] Ergin, T., Stenger, N., Brenner, P., Pendry, J.B., and Wegener, M., "Three-dimensional invisibility cloak at optical wavelengths," Science 328, 337–339 (2010).
- [3] Qi, M., Lidorikis, E., Rakich, P.T., Johnson, S.G., Joannopoulos, J.D., Ippen, E.P., and Smith, H.I., "A three-dimensional optical photonic crystal with designed point defects," Nature 429, 538–542 (2004).
- [4] Joannopoulos, J.D., Villeneuve, P.R., Fan, S.H., "Photonic crystals: Putting a new twist on light," Nature 386, 143–149 (1997).
- [5] Rinnerbauer, V., Shen, Y., Joannopoulos, J.D., Soljačić, M., Schäffler, F., and Celanovic, I., "Superlattice photonic crystal as broadband solar absorber for high temperature operation," Opt. Express 22, A1895–A1906 (2014).
- [6] Rinnerbauer, V., Lausecker, E., Schäffler, F., Reininger, P., Strasser, G., Geil, R.D., Joannopoulos, J.D., Soljačić, M., and Celanovic, I., "Nanoimprinted superlattice metallic photonic crystal as ultraselective solar absorber," Optica 2, 743–746 (2015).
- [7] Lowell, D., Lutkenhaus, J., George, D., Philipose, U., Chen, B., and Lin, Y., "Simultaneous direct holographic fabrication of photonic cavity and graded photonic lattice with dual periodicity, dual basis, and dual symmetry," Opt. Express 25, 14444–14452 (2017).
- [8] Hassan, S., Lowell, D., and Lin, Y., "High light extraction efficiency in organic light-emitting diodes by patterning the cathode in graded superlattice with dual periodicity and dual basis," J. Appl. Phys. 121, 233104 (2017).
- [9] Hassan, S., Lowell, D., Adewole, M., George, D., Zhang, H., and Lin, Y., "Extraordinary light trapping enhancement in silicon solar cell patterned with graded photonic super-crystals," Photonics 4, 50 (2017).
- [10] Lowell, D., Hassan, S., Adewole, M., Philipose, U., Chen, B., and Lin, Y., "Holographic fabrication of graded photonic super-crystals using an integrated spatial light modulator and reflective optical element laser projection system," Appl. Opt. 56, 9888–9891 (2017).
- [11] Lowell, D., Hassan, S., Sale, O., Adewole, M., Hurley, N., Philipose, U., Chen, B., and Lin, Y., "Holographic fabrication of graded photonic super-quasi-crystal with multiple level gradients," Appl. Opt. 57, 6598–6604 (2018).
- [12] Harb, A., Torres, F., Ohlinger, K., Lin, Y., Lozano, K., Di Xu, and Chen, K. P., "Holographically formed three-dimensional Penrose-type photonic quasicrystal through a lab-made single diffractive optical element," Optics Express 18, 20512-20517 (2010).
- [13] Gorkhali, S. P., Qi, J., and Grawford, G. P., "Electrically switchable mesoscale Penrose quasicrystal structure," Appl. Phys. Lett. 86, 011110 (2005).
- [14] Wang, X., Ng, C. Y., Tam, W. Y., Chan, C. T., and Sheng, P., "Large-area two-dimensional mesoscale quasi-crystals," Adv. Mater. 15, 1526–1528 (2003).
- [15] Xu, J., Ma, R., Wang, X., and Tam, W. Y., "Icosahedral quasicrystals for visible wavelengths by optical interference holography," Opt. Express 15, 4287–4295 (2007).
- [16] Zito, G., Piccirillo, B., Santamato, E., Marino, A., Tkachenko, V., and Abbate, G., "Two-dimensional photonic quasicrystals by single beam computer-generated holography," Opt. Express 16, 5164-5170 (2008).
- [17] Xavier, J., Boguslawski, M., Rose, P., Joseph, J., and Denz, C., "Reconfigurable Optically Induced Quasicrystallographic Three-Dimensional Complex Nonlinear Photonic Lattice Structures," Adv. Mat. 22, 356-360 (2010).
- [18] Arrizón, V., Sánchez de-la-Llave, D., Méndez, G., and Ulises Ruiz, "Efficient generation of periodic and quasi-periodic non-diffractive optical fields with phase holograms," Opt. Express 19, 10553-10562 (2011).
- [19] Campbell, M., Sharp, D.N., Harrison, M.T., Denning, R.G., and Turberfield, A.J., "Fabrication of photonic crystals for the visible spectrum by holographic lithography," Nature 404, 53–56 (2000).
- [20] Lin, Y., Herman, P.R., and Darmawikarta, J., "Design and holographic fabrication of tetragonal and cubic photonic crystals with phase mask: Toward the mass-production of three-dimensional photonic crystals," Appl. Phys. Lett. 86, 071117 (2005).

- [21] Chanda, D., Abolghasemi, L.E., Haque, M., Ng, M.L., and Herman, P.R., "Multi-level diffractive optics for single laser exposure fabrication of telecom-band diamond-like 3-dimensional photonic crystals," Opt. Express 16, 15402–15414 (2008).
- [22] Ohlinger, K., Zhang, H., Lin, Y., Xu, D., and Chen, K.P., "A tunable three layer phase mask for single laser exposure 3D photonic crystal generations: Bandgap simulation and holographic fabrication," Opt. Mater. Express 1, 1034–1039 (2008).
- [23] Chan, T.Y.M., Toader, O., and John, S., "Photonic band-gap formation by optical-phase-mask lithography," Phys. Rev. E 73, 046610 (2006).
- [24] Xu, D., Chen, K.P., Harb, A., Rodriguez, D., Lozano, K., and Lin, Y., "Phase tunable holographic fabrication for three-dimensional photonic crystal templates by using a single optical element," Appl. Phys. Lett. 2009 94, 231116.
- [25] George, D., Lutkenhaus, J., Lowell, D., Moazzezi, M., Adewole, M., Philipose, U., Zhang, H., Poole, Z.L., Chen, K.P., and Lin, Y., "Holographic fabrication of 3D photonic crystals through interference of multi-beams with 4 + 1, 5 + 1 and 6 + 1 configurations," Opt. Express 22, 22421–22431 (2014).
- [26] Lutkenhaus, J., Farro, F., George, D., Ohlinger, K., Zhang, H., Poole, Z., Chen, K.P., and Lin, Y., "Holographic fabrication of 3D photonic crystals using silicon based reflective optics element," Opt. Mater. Express 2, 1236–1241 (2012).
- [27] Boguslawski, M., Rose, P., and Denz, C., "Increasing the structural variety of discrete nondiffracting wave fields," Phys. Rev. A 84, 013832 (2011).
- [28] Behera, S., and Joseph, J., "Single-step optical realization of bio-inspired dual-periodic motheye and gradient-index-array photonic structures," Opt. Lett. 41, 3579–3582 (2016).
- [29] Lutkenhaus, J., George, D., Moazzezi, M., Philipose, U., and Lin, Y., "Digitally tunable holographic lithography using a spatial light modulator as a programmable phase mask," Opt. Express 21, 26227–26235 (2013).
- [30] Lutkenhaus, J., George, D., Arigong, B., Zhang, H., Philipose, U., and Lin, Y., "Holographic fabrication of functionally graded photonic lattices through spatially specified phase patterns," Appl. Opt. 53, 2548–2555 (2014).
- [31] Ohlinger, K., Lutkenhaus, J., Arigong, B., Zhang, H., and Lin, Y., "Spatially addressable design of gradient index structures through spatial light modulator based holographic lithography," J. Appl. Phys. 114, 213102 (2013).
- [32] Lutkenhaus, J., Lowell, D., George, G., Zhang, H., and Lin, Y., "Holographic Fabrication of Designed Functional Defect Lines in Photonic Crystal Lattice Using a Spatial Light Modulator," Micromachines 7, 59 (2016).
- [33] Behera, S., and Joseph, J., "Single-step optical realization of bioinspired dual-periodic motheye and gradient-index-array photonic structures," Opt. Lett. 41, 3579 (2016).
- [34] Shechtman, D., Blech, I., Gratias, D., and Cahn, J.W., "Metallic phase with long-range orientational order and no translational symmetry," Phys. Rev. Lett. 53, 1951-1953 (1984).
- [35] Levine, D., and Steinhardt, P. J., "Quasicrystals. I. Definition and structure," Phys. Rev. B 34, 596 (1986).